INTERNATIONAL JOURNAL FOR NUMERICAL METHODS IN FLUIDS
Int. J. Numer. Meth. Fluids 2009; **59**:1035–1049
Published online 10 July 2008 in Wiley InterScience (www.interscience.wiley.com). DOI: 10.1002/fld.1862

Onset of mixing layer instability in flow past a plate

Sanjay Mittal*, †

Department of Aerospace Engineering, Indian Institute of Technology Kanpur, UP 208 016, India

SUMMARY

A global stability analysis of the flow past a flat plate, normal to the flow, is carried out to determine the critical *Re* for the onset of convective instability of the mixing-layer-type modes. To suppress the primary wake mode, which leads to von Karman vortex shedding, flow past one half of the plate is studied and symmetry conditions are enforced along the wake centerline. The linearized perturbation equations for an incompressible flow are written in a moving frame of reference that travels with the perturbation and solved using a stabilized finite element method. The critical *Re* for the onset of convective instability is found to be 22, approximately, for $H=5$. Here, H is the distance of the lateral boundary from the plate centerline. Computations have also been carried out for $H=10$ and 20. The critical *Re* decreases with increase in H. Excellent agreement is observed between the results from global stability analysis and direct time integration of linearized disturbance equations. The results from the global analysis are compared with earlier reported results from local analysis of a Gaussian wake profile. Copyright © 2008 John Wiley & Sons, Ltd.

Received 3 January 2008; Revised 13 May 2008; Accepted 18 May 2008

KEY WORDS: global instability; convective instability; shear layer instability; flat plate; linear stability analysis; stabilized finite element method

1. INTRODUCTION

Bluff body flows are associated with various instabilities. It is possible to suppress the primary instability of the wake, which leads to the von Karman-type vortex shedding, by introducing a splitter plate along the wake centerline in a two-dimensional flow. Alternatively, one can consider only one half of the flow on either side of the wake centerline. Castro [1] presented results for the (in-)stability of laminar flow past a plate placed normal to the flow in a channel with slip

*Correspondence to: Sanjay Mittal, Department of Aerospace Engineering, Indian Institute of Technology Kanpur, UP 208 016, India.
†E-mail: smittal@iitk.ac.in

Contract/grant sponsor: Department of Science & Technology, India

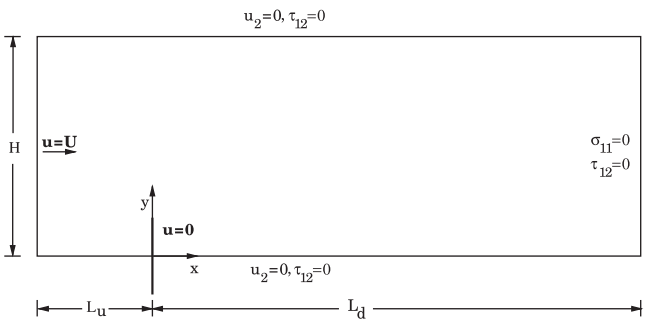

Figure 1. Flow past a flat plate of unit half-width normal to the flow: schematic of the computational domain and the boundary conditions. Only one half of the flow plane ($0 \leqslant y \leqslant H$) is computed.

walls. Symmetry conditions at the wake centerline were assumed. Only one half of the flow was considered. This, therefore, precludes the von Karman-type vortex shedding modes.

Fornberg [2] and Gajjar and Azzam [3] presented numerical results for steady flow past cylinder. Again, they utilized only one half of the domain with respect to the wake centerline. They suggest that this setup can be thought of representing a more realistic situation wherein the cylinder being considered is just one of the infinite cascade of identical cylinders located in uniform flow. Similarly, flow past one half of a plate represents a symmetric flow associated with a cascade of identical plates [1]. Figure 1 shows the schematic for such a setup. The half-width of the plate is unity. The free-stream speed, U, is used to non-dimensionalize the velocity field. All the dimensions are non-dimensionalized with half plate width. The Reynolds number, Re, is based on the half plate width and the free-stream speed.

Linear stability theory for parallel flows has been utilized in the past to understand the stability of wakes. For example, Hultgren and Aggarwal [4] considered a Gaussian wake profile given as $u^* = 1 - s\mathrm{e}^{-y^2 \ln(2)}$, where the speed is normalized by the maximum value, U_m, y is normalized by the wake's half-width and s is a measure of the level of reverse flow. They found that the critical Re for the von Karman-type modes is 3.76, while it is 53.0 for the modes when symmetry conditions are enforced on wake centerline, i.e. at $y = 0$. Interestingly, the critical Re is independent of the reverse flow parameter, s. The Re, in their study, is based on the wake half-width and the maximum velocity difference, sU_m. The stability of the mixing-layer-type modes, for symmetry conditions at wake centerline, was further studied by Castro [1]. A linear stability analysis (LSA) was carried out for various values of H. This was achieved by setting a free-slip condition on the velocity at the lateral boundary of the domain. It was found that the critical Re increases with increase in blockage. The critical Re for convective instability for $H = 100$, 10, 5 and 3 was found to be 52.99, 53.06, 57.30 and 97.11, respectively. It is noted that the results for $H = 100$ are in very good agreement with those for an unbounded domain computed by Hultgren and Aggarwal [4].

The aim of the present study is to determine the critical Reynolds number, Re_c, for the onset of convective instability via a global LSA of the non-parallel flow past a flat plate. Only one half of the plate is considered and symmetry conditions are imposed at the wake centerline. This, therefore, allows one to determine the Re_c for the onset of shear layer/mixing-layer-type modes. The value of Re_c predicted by the global LSA is confirmed via looking at the temporal growth of the energy of the disturbance field obtained from direct time integration (DTI) of the linearized

DOI: 10.1002/fld

disturbance equations (LDEs). The results from the global analysis are compared with the already available results for the local analysis of the Gaussian wake profile [1, 4].

Recently, Mittal and Kumar [5] proposed a new method to carry out the global analysis for convective instabilities in a general, non-parallel flow. In this method the equations are written in a frame of reference that moves with the disturbance. Therefore, the disturbances that are convectively unstable appear to be absolutely unstable in the moving frame. A stabilized finite element formulation is utilized to solve the disturbance equations. We utilize the same method to conduct the stability analysis for flow past a plate placed normal to the flow. The method is very general and can also be utilized to find the onset of absolute instability. In the present study we restrict our attention to convective instabilities.

The incompressible flow equations, in the velocity–pressure form, are solved via a stabilized finite element method. The stabilized formulation is based on the streamline-upwind/Petrov–Galerkin (SUPG) and pressure-stabilizing/Petrov–Galerkin (PSPG) stabilization techniques [6]. Several element-level integrals are added to the Galerkin formulation to stabilize the computations against spurious numerical oscillations. The basic Galerkin formulation is unstable for convection-dominated flows and does not allow one to use equal-order-interpolation velocity–pressure elements. The time integration of the governing flow equations is done via an implicit procedure that is second-order accurate. The time steps are chosen to adequately resolve the time-scales in the physical phenomena. The large-scale coupled non-linear equation systems resulting from the finite element discretization of the governing equations are solved iteratively by employing the generalized minimal residual (GMRES) procedure in conjunction with diagonal preconditioners.

2. THE GOVERNING EQUATIONS

2.1. The incompressible flow equations

The equations governing the flow of an incompressible fluid are given by

$$\rho\left(\frac{\partial \mathbf{u}}{\partial t}+\mathbf{u}\cdot\nabla\mathbf{u}-\mathbf{f}\right)-\nabla\cdot\boldsymbol{\sigma}=\mathbf{0} \quad \text{on } \Omega\times(0,T) \tag{1}$$

$$\nabla\cdot\mathbf{u}=0 \quad \text{on } \Omega\times(0,T) \tag{2}$$

where ρ, $\mathbf{u}$, $\mathbf{f}$ and $\boldsymbol{\sigma}$ are the density, velocity, body force and the stress tensor, respectively. For a Newtonian fluid the stress tensor is given as $\boldsymbol{\sigma}=-p\mathbf{I}+2\mu\boldsymbol{\varepsilon}(\mathbf{u})$, where $\boldsymbol{\varepsilon}$ is the strain rate given as $\boldsymbol{\varepsilon}(\mathbf{u})=\frac{1}{2}((\nabla\mathbf{u})+(\nabla\mathbf{u})^{\mathrm{T}})$. Here p and μ are the pressure and coefficient of dynamic viscosity, respectively. These equations are accompanied with appropriate boundary conditions on the velocity and stress and an initial condition on the velocity.

2.2. Linearized disturbance equations

Let the unsteady flow, $(\mathbf{u}, p)$, be expressed as a combination of the steady flow and the disturbance: $\mathbf{u}=\mathbf{U}+\mathbf{u}'$ and $p=P+p'$. Here, $(\mathbf{U}, P)$ represents the steady-state solution obtained by solving Equations (1) and (2) without the unsteady terms. $\mathbf{u}'$ and p' are the perturbation fields of the velocity and pressure, respectively. Substituting the equations for steady flow for this decomposition

DOI: 10.1002/fld

in Equations (1)–(2) and subtracting from them, one obtains the following equations for the disturbance fields:

$$\rho\left(\frac{\partial \mathbf{u}'}{\partial t}+\mathbf{u}'\cdot\nabla\mathbf{U}+\mathbf{U}\cdot\nabla\mathbf{u}'+\mathbf{u}'\cdot\nabla\mathbf{u}'\right)-\nabla\cdot\boldsymbol{\sigma}'=0 \tag{3}$$

$$\nabla\cdot\mathbf{u}'=0 \tag{4}$$

Here, $\boldsymbol{\sigma}'$ is the stress tensor due to the perturbed solution $(\mathbf{u}', p')$. We further assume that the disturbances are small and drop the non-linear term. This leads to the LDEs of the form

$$\rho\left(\frac{\partial \mathbf{u}'}{\partial t}+\mathbf{u}'\cdot\nabla\mathbf{U}+\mathbf{U}\cdot\nabla\mathbf{u}'\right)-\nabla\cdot\boldsymbol{\sigma}'=0 \tag{5}$$

$$\nabla\cdot\mathbf{u}'=0 \tag{6}$$

2.3. Global LSA

In the past, the study for convective instabilities has mostly been carried out via local analysis. The local analysis, in the context of non-parallel flows, is carried out on the velocity profiles at certain chosen stations. This method of local analysis has been applied to the wake of a cylinder [7, 8] and many other weakly non-parallel flows [9, 10]. On the other hand, several researchers have used global analysis for investigation of absolute instabilities [11–15]. Recently, Mittal and Kumar [5] proposed a method for conducting a global analysis for convective stability of non-parallel flows. They proposed that the disturbance equations be written in the frame of reference of an observer traveling with the disturbance. In this moving frame a convectively unstable flow is absolutely unstable and is, therefore, amenable to the global analysis for determining absolute (in-)stability.

Two frames of references are considered. The **x**-frame refers to the laboratory frame that is fixed to the body. The basic flow, $(\mathbf{U}, P)$, is computed in this frame. The **z**-frame moves with velocity **c** with respect to the laboratory frame. The following transformations define the changes between the two frames:

$$\mathbf{x}=\mathbf{z}+\mathbf{c}t, \quad \nabla_{\mathbf{x}}=\nabla_{\mathbf{z}}, \quad \left.\frac{\partial}{\partial t}\right|_{\mathbf{x}}=\left.\frac{\partial}{\partial t}\right|_{\mathbf{z}}-\mathbf{c}\cdot\nabla_{\mathbf{z}} \tag{7}$$

We propose a perturbation field that appears stationary with respect to the moving frame **z**. In the laboratory frame the perturbation can be expressed in the following form:

$$\mathbf{u}'(\mathbf{x},t)=\hat{\mathbf{u}}(\mathbf{x}-\mathbf{c}t)\mathrm{e}^{\lambda t}, \quad p'(\mathbf{x},t)=\hat{p}(\mathbf{x}-\mathbf{c}t)\mathrm{e}^{\lambda t} \tag{8}$$

Since the perturbation is stationary in the moving frame, its instability in this frame of reference is absolute in nature. Substituting Equation (8) into Equations (5)–(6) and using the transformations in Equation (7) we obtain

$$\rho(\lambda\hat{\mathbf{u}}+\hat{\mathbf{u}}\cdot\nabla_{\mathbf{z}}\mathbf{U}+(\mathbf{U}-\mathbf{c})\cdot\nabla_{\mathbf{z}}\hat{\mathbf{u}})-\nabla_{\mathbf{z}}\cdot\hat{\boldsymbol{\sigma}}=\mathbf{0} \quad \text{on } \Omega \tag{9}$$

$$\nabla_{\mathbf{z}}\cdot\hat{\mathbf{u}}=0 \quad \text{on } \Omega \tag{10}$$

We note that the basic flow, $\mathbf{U}(\mathbf{x})$, is computed in the laboratory frame. In the moving frame, the base flow varies with time. However, at $t=0$, $\mathbf{z}=\mathbf{x}$ and one can use the same base flow as computed

DOI: 10.1002/fld

in the stationary frame. In the moving frame, as the perturbation travels downstream it encounters a different base flow. Therefore, this analysis, for determining the global convective instability, is valid in an instantaneous sense. λ is the eigenvalue of the fluid system and governs its stability. The solution $(\mathbf{U}, P)$ is associated with a convectively unstable mode if the corresponding eigenvalue, λ, has a positive real part. The imaginary part of λ is related to the temporal frequency of the disturbance in the traveling frame. We can determine the influence of the basic flow on a perturbation traveling with various values of velocity $\mathbf{c}$. For $\mathbf{c} \neq \mathbf{0}$, the disturbance, after a sufficiently long time, is convected away. However, an unstable global mode for $\mathbf{c} = \mathbf{0}$ stays on and grows (in a linear framework). Therefore, an instability corresponding to $\mathbf{c} = \mathbf{0}$ is an absolute instability. The boundary conditions for $(\hat{\mathbf{u}}, \hat{p})$ are the homogeneous versions of the ones for $(\mathbf{U}, P)$.

3. PROBLEM SETUP

Figure 1 shows a schematic of the problem setup. The half-width of the plate is unity. The upstream and downstream boundaries are located at distances L_u and L_d from the plate, respectively. The distance between the upper boundary and the wake centerline is H. For most of the computations, in the present study, the various parameters related to the domain are $L_u = 50$, $L_d = 100$ and $H = 5$. The finite element mesh consists of 28 631 nodes and 28 050 quadrilateral elements. The plate thickness is assumed to be zero. However, two sets of nodes are created on the plate to account for the difference in the pressure on the upstream and downstream face of the plate. The element width, normal to the plate, for the elements closest to the plate is 0.04. For the unsteady computations, the time step used is 0.05.

The adequacy of the finite element mesh is demonstrated via carrying out the linear stability computations for one of the cases with a finer mesh $M2$. We refer the mesh described above as mesh $M1$. Mesh $M2$ consists of 40 386 nodes and 39 750 quadrilateral elements. The element width for this mesh, normal to the plate, for the elements closest to the plate is 0.01. For $Re = 25$ the most unstable eigenmode, computed with mesh $M2$, is associated with $\lambda_r = 0.003551$ for $c = 0.56$. The same value for the computations carried out with mesh $M1$ is 0.003544. The two meshes yield almost identical solutions. This confirms the adequacy of mesh $M1$.

Figure 1 also shows the boundary conditions used for computing the flow. Free-stream value is assigned to the velocity at the upstream boundary. At the downstream boundary, a Neumann-type boundary condition for the velocity is specified, which corresponds to zero stress vector. Along the wake centerline as well as on the upper boundary symmetry boundary conditions are employed, i.e. the component of velocity normal to and the component of stress vector along the boundary are prescribed a zero value. For the LSA and the disturbance equations, the boundary conditions on the perturbations are the homogeneous versions of the ones used for determining the steady-state solution.

4. THE FINITE ELEMENT FORMULATION

4.1. The incompressible flow equations

Consider a finite element discretization of the domain, Ω, into subdomains Ω^e, $e = 1, 2, \ldots, n_{el}$, where n_{el} is the number of elements. Based on this discretization, let $\mathscr{S}^h_{\mathbf{u}}$ and $\mathscr{S}^h_p$ be the

DOI: 10.1002/fld

finite element trial function spaces for velocity and pressure, respectively, and $\mathscr{V}_{\mathbf{u}}^h$ and $\mathscr{V}_p^h$ be the weighting function spaces. The stabilized finite element formulation of Equations (1)–(2) is expressed as follows: find $\mathbf{u}^h \in \mathscr{S}_{\mathbf{u}}^h$ and $p^h \in \mathscr{S}_p^h$ such that $\forall \mathbf{w}^h \in \mathscr{V}_{\mathbf{u}}^h$, $q^h \in \mathscr{V}_p^h$

$$\int_\Omega \mathbf{w}^h \cdot \rho \left(\frac{\partial \mathbf{u}^h}{\partial t} + \mathbf{u}^h \cdot \nabla \mathbf{u}^h - \mathbf{f} \right) \mathrm{d}\Omega + \int_\Omega \boldsymbol{\varepsilon}(\mathbf{w}^h) : \boldsymbol{\sigma}(p^h, \mathbf{u}^h) \, \mathrm{d}\Omega$$
$$+ \int_\Omega q^h \nabla \cdot \mathbf{u}^h \, \mathrm{d}\Omega + \sum_{e=1}^{n_{\mathrm{el}}} \int_{\Omega^e} \frac{1}{\rho} (\tau_{\mathrm{SUPG}} \rho \mathbf{u}^h \cdot \nabla \mathbf{w}^h + \tau_{\mathrm{PSPG}} \nabla q^h)$$
$$\cdot \left[\rho \left(\frac{\partial \mathbf{u}^h}{\partial t} + \mathbf{u}^h \cdot \nabla \mathbf{u}^h - \mathbf{f} \right) - \nabla \cdot \boldsymbol{\sigma}(p^h, \mathbf{u}^h) \right] \mathrm{d}\Omega^e$$
$$+ \sum_{e=1}^{n_{\mathrm{el}}} \int_{\Omega^e} \tau_{\mathrm{LSIC}} \nabla \cdot \mathbf{w}^h \rho \nabla \cdot \mathbf{u}^h \, \mathrm{d}\Omega^e = \int_{\Gamma_h} \mathbf{w}^h \cdot \mathbf{h}^h \, \mathrm{d}\Gamma \tag{11}$$

where Γ_g and Γ_h are complementary subsets of the boundary Γ on which Dirichlet and Neumann-type boundary conditions are assigned as follows:

$$\mathbf{u} = \mathbf{g} \quad \text{on } \Gamma_g, \quad \mathsf{n} \cdot \boldsymbol{\sigma} = \mathbf{h} \quad \text{on } \Gamma_h \tag{12}$$

where n is the unit normal vector to Γ_h. In the variational formulation given in Equation (11), the first three terms and the right-hand side constitute the Galerkin formulation of the problem. It is well known that the Galerkin formulation is unstable with respect to the advection operator as the cell Reynolds number (based on the local flow velocity and mesh size) becomes larger. In addition, not all combinations of the velocity and pressure interpolations are admissible in the Galerkin formulation. Elements that do not satisfy the Babuska–Brezzi condition lead to oscillatory solutions and, sometimes, no solution at all. To give stability to the basic formulation, a series of element-level integrals are added. The first series of element-level integrals are the SUPG and PSPG stabilization terms added to the variational formulations [6]. The SUPG formulation for convection-dominated flows was introduced by Hughes and Brooks [16] and Brooks and Hughes [17]. The Petrov–Galerkin term for Stokes flows, to admit the use of equal-order interpolations for velocity and pressure without producing oscillations in the pressure field, was proposed by Hughes *et al.* [18]. Tezduyar *et al.* [6] proposed a formulation using the SUPG and PSPG stabilizations for finite Reynolds number flows. The second series of element-level integrals are stabilization terms based on the least squares of the divergence-free condition on the velocity field. The definition for τ_{PSPG} and τ_{SUPG} is given by the following relations based on its values for the advection and diffusion limits:

$$\tau_{\mathrm{SUPG}} = \tau_{\mathrm{PSPG}} = \left(\frac{1}{\tau_{\mathrm{ADV}}^2} + \frac{1}{\tau_{\mathrm{DIF}}^2} \right)^{-1/2} \tag{13}$$

where

$$\tau_{\mathrm{ADV}} = \frac{h^e}{2\|\mathbf{u}^h\|}, \quad \tau_{\mathrm{DIF}} = \frac{(h^e)^2}{12\nu} \tag{14}$$

Here, h^e is the element length and various definitions have been used by researchers in the past. Mittal [19] conducted a systematic numerical study to investigate the effect of high aspect ratio

DOI: 10.1002/fld

elements on the performance of the finite element formulation for three commonly used definitions of h^e. In this paper we use the definition based on the minimum edge length of an element. The coefficient τ_{LSIC} is defined as

$$\tau_{\mathrm{LSIC}} = \left(\frac{1}{\delta_{\mathrm{ADV}}^2} + \frac{1}{\delta_{\mathrm{DIF}}^2} \right)^{-1/2} \tag{15}$$

where

$$\delta_{\mathrm{ADV}} = \frac{h^e \|\mathbf{u}^h\|}{2}, \quad \delta_{\mathrm{DIF}} = \frac{(h^e)^2 (\|\mathbf{u}^h\|)^2}{12\nu} \tag{16}$$

The non-linear equation system resulting from the finite element discretization of the flow equations is solved using the GMRES technique [20] in conjunction with diagonal preconditioners. The implicit method used in the present study allows us to seek steady-state solutions by simply dropping the unsteady terms in the governing equations.

4.2. The linear stability equations

Let $\hat{\mathscr{S}}_{\mathbf{u}}^h$ and $\hat{\mathscr{S}}_p^h$ be the finite element trial function spaces and $\hat{\mathscr{V}}_{\mathbf{u}}^h$ and $\hat{\mathscr{V}}_p^h$ the weighting function spaces for the perturbations in the velocity and pressure fields, respectively. The finite element formulation for the perturbation equations, (9) and (10), is given as follows: find $\hat{\mathbf{u}}^h \in \hat{\mathscr{S}}_{\mathbf{u}}^h$ and $\hat{p}^h \in \hat{\mathscr{S}}_p^h$ such that $\forall \hat{\mathbf{w}}^h \in \hat{\mathscr{V}}_{\mathbf{u}}^h$ and $\hat{q}^h \in \hat{\mathscr{V}}_p^h$

$$\begin{aligned}
&\int_\Omega \hat{\mathbf{w}}^h \cdot \rho(\lambda \hat{\mathbf{u}}^h + (\mathbf{U}^h - \mathbf{c}) \cdot \nabla \hat{\mathbf{u}}^h + \hat{\mathbf{u}}^h \cdot \nabla \mathbf{U}^h)\, \mathrm{d}\Omega + \int_\Omega \boldsymbol{\varepsilon}(\hat{\mathbf{w}}^h) : \boldsymbol{\sigma}(\hat{p}^h, \hat{\mathbf{u}}^h)\, \mathrm{d}\Omega \\
&+ \int_\Omega \hat{q}^h \nabla \cdot \hat{\mathbf{u}}^h \, \mathrm{d}\Omega + \sum_{e=1}^{n_{\mathrm{el}}} \int_{\Omega^e} \frac{1}{\rho} (\tau_{\mathrm{SUPG}} \rho (\mathbf{U}^h - \mathbf{c}) \cdot \nabla \hat{\mathbf{w}}^h + \tau_{\mathrm{PSPG}} \nabla \hat{q}^h) \\
&\cdot [\rho(\lambda \hat{\mathbf{u}}^h + (\mathbf{U}^h - \mathbf{c}) \cdot \nabla \hat{\mathbf{u}}^h + \hat{\mathbf{u}}^h \cdot \nabla \mathbf{U}^h) - \nabla \cdot \boldsymbol{\sigma}(\hat{p}^h, \hat{\mathbf{u}}^h)]\, \mathrm{d}\Omega^e \\
&+ \sum_{e=1}^{n_{\mathrm{el}}} \int_{\Omega^e} \tau_{\mathrm{LSIC}} \nabla \cdot \hat{\mathbf{w}}^h \rho \nabla \cdot \hat{\mathbf{u}}^h \, \mathrm{d}\Omega^e = 0
\end{aligned} \tag{17}$$

The stabilization coefficients for the LSA are given by the same definition as defined in Equations (13)–(16) except that they are based on the steady-state velocity field $\mathbf{U}^h$. Equation (17) leads to a generalized eigenvalue problem of the form $\mathbf{A}X - \lambda \mathbf{B}X = 0$, where $\mathbf{A}$ and $\mathbf{B}$ are non-symmetric matrices. In this study we use the shift-invert transformation in conjunction with the subspace iteration method [21] to track the eigenvalue with the largest real part.

5. RESULTS

5.1. The steady flow

First, the steady flow is computed for various Re by dropping the time-dependent terms from Equations (1)–(2). Figure 2 shows the vorticity field and the streamlines in the recirculation region for the $Re = 25$ and 100 flow. The length of the recirculation bubble at these two values

DOI: 10.1002/fld

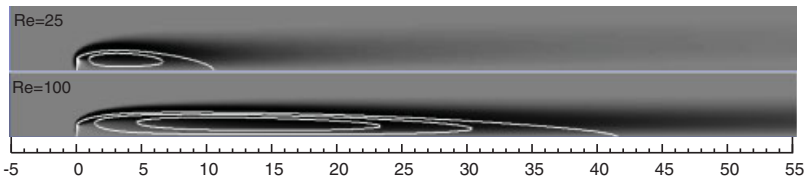

Figure 2. $Re = 25, 100$ steady flow past a flat plate: vorticity field and streamlines in the recirculation region.

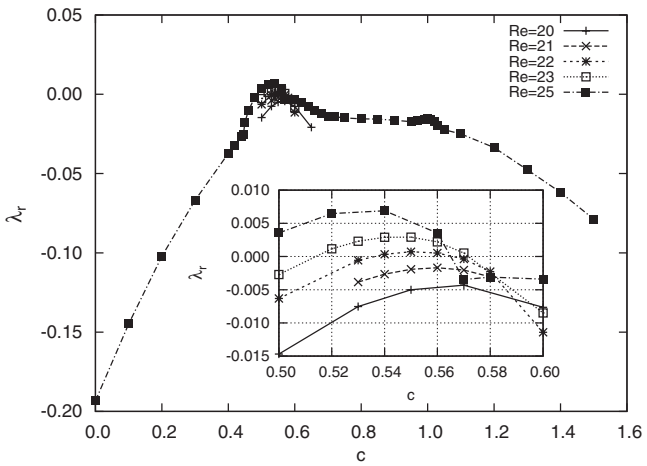

Figure 3. Flow past a flat plate: real part of the eigenvalue corresponding to the most unstable eigenmode for various c and Re.

of Re is ~ 10.5 and 41.5 units, respectively. Very good agreement is observed with the results from other researchers [22]. In all the figures in this paper, the shading in the grey scale represents vorticity. Darker shades, with respect to the background, refer to negative values, whereas the lighter shades of grey represent positive vorticity values.

5.2. *Linear stability analysis*

Once the steady-state solution is available, at each Re, the stability analysis is carried out for various values of **c**. In general, the perturbation can travel in any direction. However, in the present computations **c** is restricted to the streamwise direction. Therefore, in the remainder of this paper we refer to it simply by a scalar c.

5.2.1. Critical Re for convective instability. Figure 3 shows the variation in the real part of eigenvalue for the most unstable eigenmode for various Re and speed of the disturbance. At the critical Re, for the onset of convective instability, the real part of the eigenvalue, λ_r, changes the sign to a positive value for some value of c. At $Re = 21$ and lesser λ_r is less than zero for all values of c. The $Re = 22$ flow appears to be marginally unstable for values of c lying between 0.54 and 0.56, approximately. Therefore, for this flow with $H = 5$, the critical Re for the onset of convective instability is approximately 22. At the onset of the instability λ_i is found to be 0.

DOI: 10.1002/fld

Figure 4. $Re=25$ flow past a flat plate: vorticity field for the most unstable eigenmode for various c. The grey scale key is also shown (right).

5.2.2. $Re=25$ flow. Figure 3 shows the real part of the eigenvalue corresponding to the most unstable mode for various values of c. Clearly, the $Re=25$ flow is absolutely stable since the most unstable mode is associated with a negative real eigenvalue for $c=0$. λ_r increases with increase in c and achieves a positive value for a small range of disturbance speed. Maximum instability is observed for the disturbance traveling at $c\sim0.54$. The flow regains stability for disturbances traveling at a speed greater than $c\sim0.57$. Another peak in the variation in λ_r is observed for $c\sim1$. However, the flow remains stable to all these disturbances.

Figure 4 shows the vorticity field for the most unstable modes corresponding to various speeds of the disturbance. The modes associated with $c\sim0.5$ are mostly active in the near wake region ($x<20$) and are reminiscent of the instability of the shear/mixing layer.

5.3. DTI of the LDEs

To investigate the correctness of the results predicted from the proposed global stability analysis, a DTI of the LDEs is conducted. An instantaneous disturbance is introduced in the flow at $t=0$. The y component of the velocity disturbance at a node lying next to the plate in the near wake $(0.04, 0.6)$ is assigned a value of 0.1 at $t=0$.

5.3.1. $Re=25$ flow. The time evolution of the vorticity field for $Re=25$ flow with the introduction of a point disturbance is shown in Figure 5. The similarity between the disturbance field for $t<20$ and the most unstable eigenmodes, shown in Figure 4, for $0.5\leqslant c\leqslant0.6$ can be clearly observed. The speed of the disturbance from the location of the vortex structures at various time instants is estimated to be $c\sim0.55$. This is in very good agreement with the c for which the fastest growing mode is observed from the global LSA.

5.3.2. Estimation of the critical Re. DTI of the LDEs is conducted for other values of Re. We define the energy of the disturbance in the computational domain as $E(t)=1/2\int_\Omega \mathbf{u}'\cdot\mathbf{u}'\,d\Omega$. The time evolution of the normalized energy of the disturbance, $E(t)/E(0)$, is shown in Figure 6. $E(0)$ is the energy of the imposed disturbance at $t=0$.

DOI: 10.1002/fld

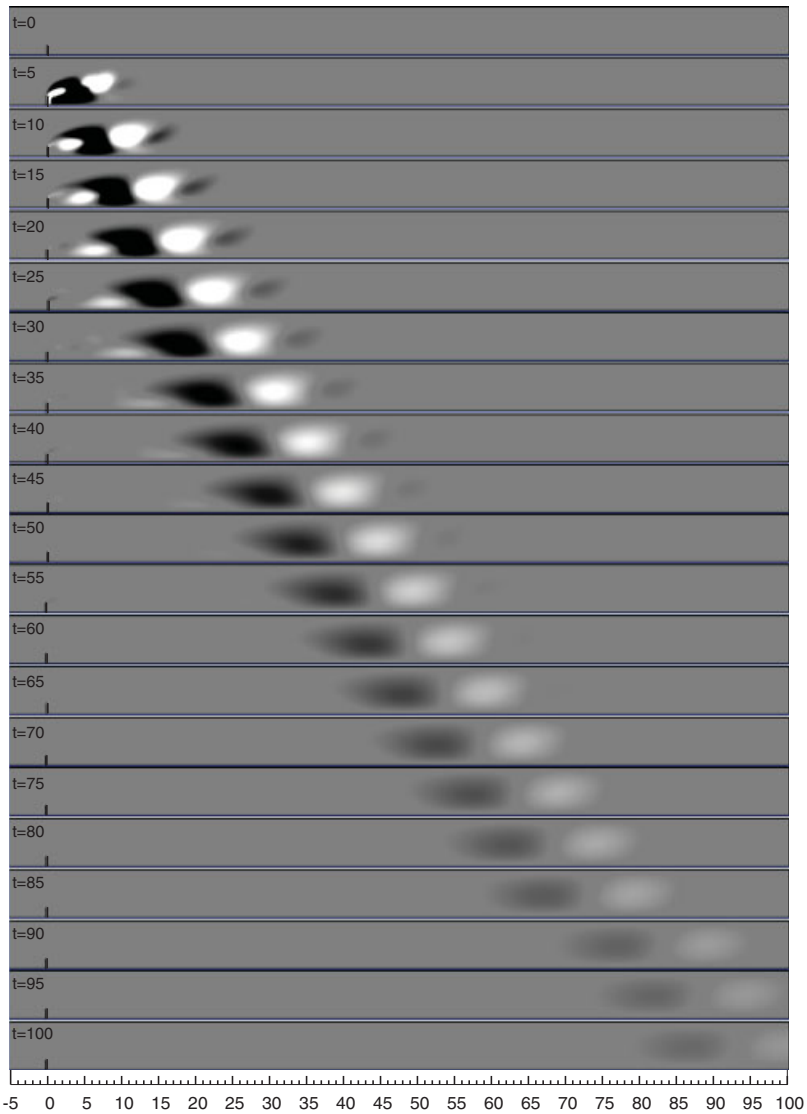

Figure 5. $Re=25$ flow past a flat plate obtained by direct time integration of the linearized disturbance equations: time evolution of the vorticity field. An instantaneous disturbance is introduced in the flow at $t=0$, which corresponds to assigning the y component of the velocity disturbance at $(0.04, 0.6)$ a value of 0.1. The dark shades of grey (compared with the background) represent negative vorticity, whereas the lighter shades indicate positive vorticity.

For $Re \leqslant 21$ the energy of the disturbance field decreases monotonically with t. However, a local peak in the energy is observed for $Re \geqslant 23$. This is more clear from the close-up view shown in Figure 6. For $Re=21$ and lesser, the flow is convectively stable and, therefore, a monotonic decrease in energy with time is observed. For $Re=23$ and higher, the disturbance, for a certain period of time, is amplified as it convects downstream. This leads to an increase in the energy

DOI: 10.1002/fld

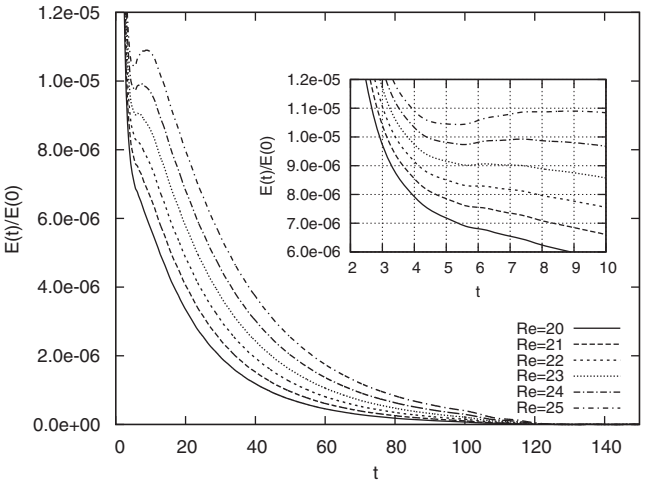

Figure 6. Flow past a flat plate obtained by direct time integration of the linearized disturbance equations: time evolution of the normalized energy field. An instantaneous disturbance is introduced in the flow at $t=0$, which corresponds to assigning the y component of the velocity disturbance at $(0.04, 0.6)$ a value of 0.1.

during this time interval. However, the flow is absolutely stable in this range of Re. Therefore, the energy of the disturbance field in this finite domain settles down to zero (machine level zero of the order of 10^{-14}) after sufficiently long time. We note that the LSA predicts $Re_c \sim 22$ while the computations from DTI show that the critical Re is closer to 23. We believe that the results from LSA are expected to be more accurate than DTI of the linearized equation. In linear DTI an impulsive disturbance introduced at $t=0$ excites many modes of the flow. For Re that is very slightly larger than Re_c it is expected that only one mode is convectively unstable while all others are stable. Therefore, even though the energy related to the unstable mode will grow with time, it may get overcompensated by the decay of energy of all other stable modes. Thus, the linear DTI in conjunction with the introduction of an impulsive disturbance can overpredict the critical Re.

To see this more clearly, we repeat the DTI of the linearized equation with a different set of initial conditions. The computations are initiated with the real part of the most unstable eigenmode, obtained from the global stability analysis at that Re. The time evolution of the normalized energy of the disturbance, $E(t)/E(0)$, is shown in Figure 7. From this figure it is very clear that at $t=0^+$ the energy of the $Re=21$ flow decreases while it increases for $Re=22$ and higher. At $Re=22$ the increase in energy is very marginal as seen from the close-up view in Figure 7. From this we conclude that the critical Re is close to 22 as predicted by the LSA. The excellent agreement between the results from the global LSA and DTI of the LDEs confirms the correctness of the results.

5.4. Comparison with results from local analysis

Hultgren and Aggarwal [4] considered a Gaussian wake profile given as $u^* = 1 - s e^{-y^2 \ln(2)}$, where the speed is normalized by the maximum value, y is normalized by the wake's half-width and s is a measure of the level of reverse flow. They used the linear stability theory for parallel flows to analyze the stability of this profile. It was found that the critical Re for the von Karman-type modes is 3.76 while it is 53.0 for the modes when symmetry conditions are enforced on wake

DOI: 10.1002/fld

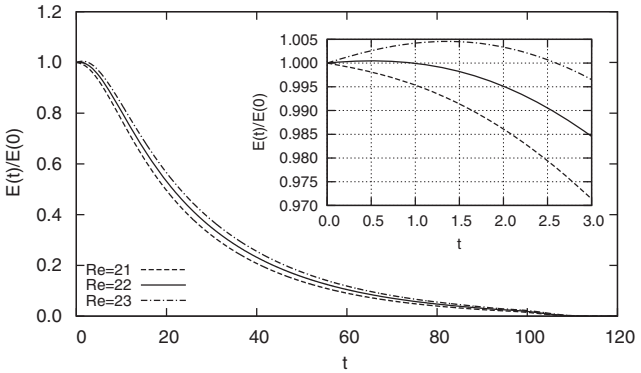

Figure 7. Flow past a flat plate obtained by direct time integration of the linearized disturbance equations: time evolution of the normalized energy field. The real part of the rightmost eigenmode obtained from global linear stability analysis at each Re, and for that value of c at which the flow is convectively most unstable, is used as an initial condition.

centerline, i.e. at $y=0$. Interestingly, the critical Re is independent of the reverse flow parameter s. The Re, in their study, is based on the wake half-width and the maximum velocity difference. The stability of the mixing-layer-type modes, for symmetry conditions at wake centerline, was further studied by Castro [1]. An LSA was carried out for various values of H. This was achieved by setting a free-slip condition on the velocity at the lateral boundary of the domain. It was found that the critical Re for $H=100$, 10, 5 and 3 is 52.99, 53.06, 57.30 and 97.11, respectively.

We now compare our results from the global stability analysis of the non-parallel flow with the ones from the local analysis of the parallel flow from Castro [1]. Recall that the present analysis results in a $Re_c \sim 22$. For the $Re=22$ flow we estimate the local Reynolds number, Re_l, in the wake based on the local wake half-width and the maximum velocity difference. Figure 8 shows the stream wise variation in the effective value of the reverse flow parameter, $s(x)$, half wake width and Re_l. The parameter $s(x)$ is computed using the expression $s(x)=(u(x, y=H)-u(x, y=0))/u(x, y=H)$, whereas Re_l is calculated based on the wake half-width at each x location and the maximum speed difference given by $s(x)u(x, y=H)$. The wake half-width, $b(x)$, is the vertical distance from the wake centerline where the velocity defect with respect to $u(x, y=H)$ is one-half the maximum defect at each location $(=u(x, H)-u(x, 0))$. We note that there is a substantial variation in Re_l and that it achieves a maximum value of 60.66 at $x=3.82$. The local analysis of the Guassian profile underpredicts the Re_c slightly. Castro [1] found this value to be 57.30 for $H=5$. The difference in the two sets of results is less than 6%.

To investigate the reason for the fair agreement between the results from the local and global analysis, we compare the velocity profiles of the steady flow obtained from direct numerical simulation with the Gaussian profile used by Castro [1] and Hultgren and Aggarwal [4]. Figure 9 shows the two sets of velocity profiles. The Gaussian profile, $u_G(x, y)$, has been plotted by utilizing the $s(x)$ and $b(x)$ from the steady-state data. The following expression has been used:

$$u_G(x, y)=u(x, y=H)[1-s(x)\mathrm{e}^{-(y/b(x))^2 \ln(2)}] \tag{18}$$

From Figure 9 it can be observed that except in the very near wake ($x<3$), the Gaussian profile is a good approximation to the velocity profile in the wake region. That, perhaps, explains the

DOI: 10.1002/fld

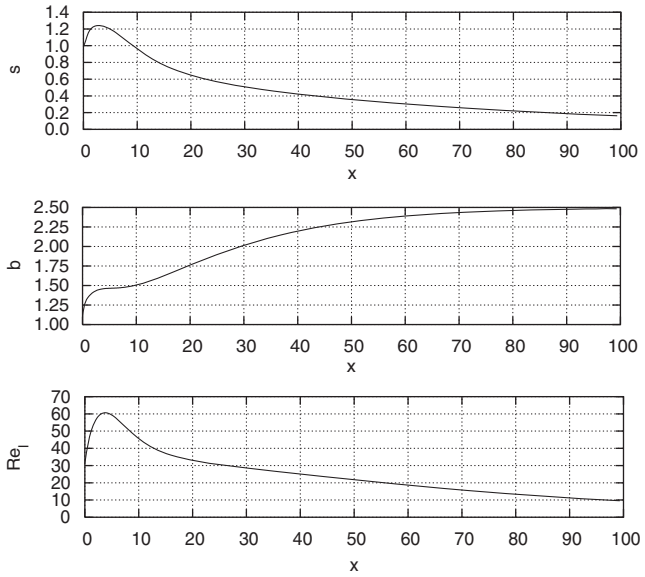

Figure 8. $Re=22$ steady flow past a flat plate: stream wise variation in the effective value of $s(x)=(u(x, y=H)-u(x, y=0))/u(x, y=H))$, half wake width and the local Reynolds number, Re_l, based on $s(x)u(x, y=H)$ and b.

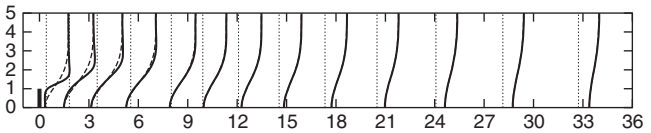

Figure 9. $Re=22$ steady flow past a flat plate: velocity profiles at various streamwise locations shown in solid lines. Also shown in broken lines are the profiles assuming a Gaussian mean profile given by Equation (18). For reference, the plate is shown in the thick solid line and $u=0$ in the dotted line.

success of the local analysis in predicting a reasonable approximation to the critical Re for the onset of convective instability of mixing layer modes for the normal flat plate.

5.5. *Effect of H*

From the analysis of the Gaussian wake profile, Hultgren and Aggarwal [4] found that the critical Re for the shear layer mode is 53.0. The stability of the mixing-layer-type modes was further studied by Castro [1]. An LSA was carried out for various values of H. This was achieved by setting a free-slip condition on the velocity at the lateral boundary of the domain. The critical Re for $H=100$, 10, 5 and 3 was found to be 52.99, 53.06, 57.30 and 97.11, respectively. It is observed that the critical Re increases with decrease in H. Figure 10 shows the variation in the real part of eigenvalue for the most unstable eigenmode for various Re and speed of the disturbance for $H=10$ and 20. The critical Re for the onset of instability is ~ 19 and 17.3 for $H=10$ and 20, respectively. As was observed by Castro [1], the critical Re decreases with increase in H.

DOI: 10.1002/fld

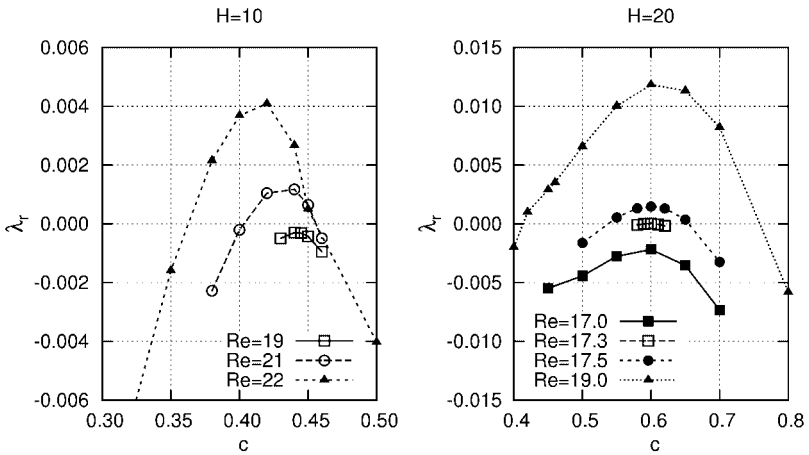

Figure 10. Flow past a flat plate: real part of the eigenvalue corresponding to the most unstable eigenmode for various c and Re for $H=10$ (left) and $H=20$ (right).

6. CONCLUSION

Global LSA of the flow past a normal flat plate has been carried out. The investigation is restricted to symmetric modes of instability to preclude the von Karman-type of vortex shedding modes. Therefore, only half of the plate is considered and symmetry conditions are applied at the wake centerline. Most of the computations have been carried out for $H=5$. The critical Re for the onset of convective instability is found to be approximately 22 and relates to the instability of the separated mixing/shear layer. The results from the global LSA are in excellent agreement with those from DTI of the LDEs. The disturbance field from the DTI appears to be quite similar to the most unstable mode from LSA. Good match is also seen between the two sets of results for the speed of propagation of the disturbance. The effect of blockage has also been investigated. It is found that the critical Re, for the onset of the instability, decreases as the lateral boundary of the domain is moved farther away. Re_c is $\sim$22, 19 and 17.3 for $H=5$, 10 and 20, respectively.

The results are compared with the ones from local analysis of the Gaussian wake profile carried out by researchers, earlier. The Re_c from the local analysis is 57.3. However, this value is based on the wake half-width and the difference between the minimum and maximum speeds. The $Re=22$ steady flow from the direct numerical simulation is investigated to study the streamwise variation in the wake profiles. The wake half-width and the difference between the minimum and maximum speeds, at each streamwise station, vary quite significantly leading to a large variation in the local Reynolds number, Re_l. The peak value of Re_l is 60.66 and is achieved at $x=3.82$. The difference in the critical Re_l from the local and global analyses is close to 6%. Further, it is found that except in the near wake ($x<3$) the velocity profiles are very similar to the Gaussian wake profile. The reasonably good prediction by the local analysis can be attributed to the similarity of the velocity profiles in the wake of the plate to the Gaussian wake profile. Unlike the local analysis, the global analysis provides the global mode shape.

DOI: 10.1002/fld

ACKNOWLEDGEMENTS

Partial support for this study from the Department of Science & Technology, India, is gratefully acknowledged.

REFERENCES

1. Castro IP. The stability of laminar symmetric separated wakes. *Journal of Fluid Mechanics* 2005; **532**:389–411.
2. Fornberg B. Steady incompressible flow past a row of circular cylinders. *Journal of Fluid Mechanics* 1991; **225**:655–671.
3. Gajjar JSB, Azzam N. Numerical solution of the Navier–Stokes equations for the flow in a cylinder cascade. *Journal of Fluid Mechanics* 2004; **520**:51–82.
4. Hultgren LS, Aggarwal AK. Absolute instability of the Gaussian wake profile. *Physics of Fluids* 1987; **30**: 3383–3387.
5. Mittal S, Kumar B. A stabilized finite element method for global analysis of convective instabilities in nonparallel flows. *Physics of Fluids* 2007; **19**:088105.
6. Tezduyar TE, Mittal S, Ray SE, Shih R. Incompressible flow computations with stabilized bilinear and linear equal-order-interpolation velocity–pressure elements. *Computer Methods in Applied Mechanics and Engineering* 1992; **95**:221–242.
7. Yang X, Zebib A. Absolute and convective instability of a cylinder wake. *Physics of Fluids A* 1989; **1**:689–696.
8. Monkewitz PA. The absolute and convective nature of instability in two-dimensional wakes at low Reynolds numbers. *Physics of Fluids* 1988; **31**:999–1006.
9. Pierrehumbert RT. Local and global baroclinic instability of zonally varying flow. *Journal of the Atmospheric Sciences* 1985; **41**:2141–2162.
10. Huerre P, Chomaz JM, Redekopp LG. Bifurcations to local and global modes in spatially developing flows. *Physical Review Letters* 1988; **60**:25–28.
11. Cliffe KA, Winters KH, Jackson CP. *The Prediction of Instabilities Using Bifurcation Theory*. Wiley: New York, 1986.
12. Jackson CP. A finite-element study of the onset of vortex shedding in flow past variously shaped bodies. *Journal of Fluid Mechanics* 1987; **182**:23–45.
13. Morzynski M, Thiele F. Numerical stability analysis of a flow about a cylinder. *Zeitschrift für Angewandte Mathematik und Mechanik* 1991; **71**:T424–T428.
14. Morzynski M, Afanasiev K, Thiele F. Solution of the eigenvalue problems resulting from global non-parallel flow stability analysis. *Computer Methods in Applied Mechanics and Engineering* 1999; **169**:161–176.
15. Ding Y, Kawahara M. Three dimensional linear stability analysis of incompressible viscous flows using the finite element method. *International Journal for Numerical Methods in Fluids* 1999; **31**:451–479.
16. Hughes TJR, Brooks AN. A multi-dimensional upwind scheme with no crosswind diffusion. In *Finite Element Methods for Convection Dominated Flows*, vol. 34, Hughes TJR (ed.). ASME: New York, 1979; 19–35.
17. Brooks AN, Hughes TJR. Streamline upwind/Petrov–Galerkin formulations for convection dominated flows with particular emphasis on the incompressible Navier–Stokes equations. *Computer Methods in Applied Mechanics and Engineering* 1982; **32**:199–259.
18. Hughes TJR, Franca LP, Balestra M. A new finite element formulation for computational fluid dynamics: V. Circumventing the Babuška–Brezzi condition: a stable Petrov–Galerkin formulation of the Stokes problem accommodating equal-order interpolations. *Computer Methods in Applied Mechanics and Engineering* 1986; **59**:85–99.
19. Mittal S. On the performance of high aspect-ratio elements for incompressible flows. *Computer Methods in Applied Mechanics and Engineering* 2000; **188**:269–287.
20. Saad Y, Schultz M. GMRES: a generalized minimal residual algorithm for solving nonsymmetric linear systems. *SIAM Journal on Scientific and Statistical Computing* 1986; **7**:856–869.
21. Stewart GW. Methods of simultaneous iteration for calculating eigenvectors of matrices. In *Topics in Numerical Analysis II*, Miller JHH (ed.). Academic Press: New York, 1975; 169–185.
22. Castro IP. Weakly stratified laminar flow past normal flat plates. *Journal of Fluid Mechanics* 2002; **454**:21–46.

DOI: 10.1002/fld